Development of methods for deconvolution algorithms performance analysis using FIJI and Icy plugins

Luciana A. Erbes*[a,b], Ángel A. Zeitoune[a,b], Víctor H. Casco[b], Javier Adur[a,b]
[a]Biofotónica y Procesamiento de Información Biológica (ByPIB), CITER - Centro de Investigación y Transferencia de Entre Ríos, CONICET-UNER, Argentina; [b]Microscopy Laboratory Applied to Molecular and Cellular Studies (LAMAE), FI-UNER, Ruta Provincial 11 Km. 10, Oro Verde, Entre Ríos, Argentina.

ABSTRACT

The analysis of deconvolution algorithms performance is crucial when is wanted to use deconvolution as an effective image restoration approach. The performance of deconvolution algorithms available in Open Source software was compared by using three-dimensional (3D) microscopy images. DeconvolutionLab and MitivBlindDeconvolution were the plugins chosen from FIJI and Icy respectively. In the first place, analyses included 3D bead stack measurements both pre- and post-deconvolution by using theoretical and empirical Point Spread Functions (PSFs) as well as parameter variation. The set of parameters that resulted in the improvement of both the 3D morphology and intensity of the beads was applied to 3D autofluorescence colon tissue images from BALB/c mice to evaluate if original morphology and intensity features were restored.

Keywords: deconvolution, algorithms, PSF, FIJI, Icy

1. INTRODUCTION

Images obtained by conventional fluorescence microscopy contain light from throughout the specimen. Thereby, the reduction of out-of-focus signal is a task of 3D microscopy. In a confocal microscope, this reduction is achieved by positioning a pinhole in front of the detector, such that most of the light passing through the pinhole derives from the focal plane and not from surrounding regions[1]. This results in excellent optical sections from thick specimens, but because a considerable percentage of the light is rejected by the pinhole, the signal may be weakened[2]. There are different ways to computationally reduce the out-of-focus light by deconvolution microscopy. Since its introduction in 1983, deconvolution microscopy has become a key image processing tool for visualizing the cellular structures of fixed and living specimens in three dimensions and at sub-resolution scale[3]. Processing of 3D data sets from wide-field microscopy is the most common use[2]. Deconvolution methods use a characterization of the out-of-focus light based on the 3D image of a point source of light, the so-called point-spread function (PSF), which is specific for the optical system. It is used to infer the original distribution of point sources in a specimen that must have given rise to the image collected[1].

The computational 3D image deconvolution techniques can be categorized into six broad classes: no-neighbor, neighbouring, linear, nonlinear, statistical methods, and blind deconvolution[4]. Some of them have been developed in different plugins by commercial and Open Source packages such us Huygens[5], AutoQuant[6], ImageJ[7], FIJI[8] and Icy[9]. Nowadays, deconvolution is a heavy computational method accessible to any laboratory, thanks to the astonishing progress of computer science. A stack of images can now be processed by inexpensive computers, in a time period as short as a few milliseconds to a few hours, depending on acquisition size and the deconvolution algorithm used[3]. Despite the effort to provide user-friendly solutions, deconvolution remains a challenging task and specially should be taken into consideration the choice of a good software, the right algorithm and the correct settings[10].

*lerbes@bioingenieria.edu.ar; phone +54 (343) 4975-100/101 – 120.

12th International Symposium on Medical Information Processing and Analysis, edited by Eduardo Romero, Natasha Lepore, Jorge Brieva, Ignacio Larrabide, Proc. of SPIE Vol. 10160, 101600I
 · doi: 10.1117/12.2255820

The deconvolution algorithm performance analysis is an extremely important step in order to apply deconvolution as an effective image restoration technique. There are many deconvolution plugins from Open Source software such as the widely used DeconvolutionLab[11] and the rather new MitivBlindDeconvolution[12]. At the same time, they have a set of parameters to be established. The main obstacle is not to find a deconvolution algorithm but to choose and apply one, being confident about its performance. Because of that, the main goal of this work was to develop a procedure to compare deconvolution outcomes of algorithms by acquiring post-deconvolution measurements about size and intensity of 3D wide-field microscopy bead images. Then, the set of algorithm, parameters and PSF that presented better performance were applied to 3D colon tissue stacks in order to analyze colon crypts structures. According to our experience, digital deconvolution methods properly applied are essential to enable the achievement of suitable quantification analyses.

2. MATERIALS AND METHODS

2.1 Analyzed deconvolution algorithms

Four deconvolution algorithms were selected from FIJI for the comparison procedure. All of them belong to the DeconvolutionLab plugin, namely: Landweber[13], Tikhonov-Miller[14], Richardson-Lucy[14] and Richardson-Lucy with total variation (TV) regularization[15]. Additionally, a development of blind deconvolution method was selected from the MitivBlindDeconvolution plugin, recently available in Icy. In both cases, the plugins have the possibility to modify some parameters, such as iterations, positivity constraint and regularization parameter.

2.2 PSFs

Two theoretical PSFs were developed for the optical system in use. One of them was calculated through a formula that uses a first-order Bessel function (Castleman, 1996[16]) and the other was calculated by the MitivBlindDeconvolution plugin. Furthermore, an empirical PSF was obtained by using fluorescent microspheres (F-8888 kit, Molecular Probes[17]).

2.3 Analyzed images

3D images of fluorescent microspheres (4 μm), as patron of known shape and size, were used to test the deconvolution algorithms. Then, 3D tissue images were acquired from mouse BALB/C non-pathological colon samples and chemically-induced colon cancer (Azoxymethane/Dextran Sodium Sulphate), (Bianchi et al., 2013[18]). Stacks were obtained by optical sectioning by using a digital deconvolution microscope[19] based on an Olympus BX50 system (UPlanApo 40X, 0.85 NA and 20X, 0.7 NA, objective lens). Samples were excited with a mercury UV lamp for epifluorescence microscopy (U-MWIB (BP 460-490, DM 505, BA 515) and U-MSWG cube filters (BP 480-550, DM 570, BA 590)). Images were recorded by using an Apogee cooled monochromatic charge-coupled device (CCD) camera (14 bits of resolution with a 9 μm^2 pixel size), and saved in 8 bit .tiff files. Each stack was made up of 40 optical sections (512x512 $pixel^2$) with 0.5 μm per optical section. A 0.5X demagnification lens was set for bead image acquisitions.

2.4 Parameters tested in deconvolution

In order to evaluate the deconvolution algorithms performance, pre- and post-deconvolution measurements were set to compare changes. Morphology (estimated diameter in XY-plane and Full Width at Half Maximum (FWHM) in Z-plane), intensity (maximum intensity in XY and Z-plane) and proximity (distance between maximum intensity values from each bead) parameters were measured. Pre-deconvolution measurements were obtained by a specific macro developed to verify the beads deformation both in XY and Z-planes after optical sectioning. Those values were used to compare the performance of the deconvolution algorithms.

3. RESULTS

3.1 Procedure to analyze FIJI's deconvolution algorithms through the morphology of the beads

A FIJI macro (depicted both in the chart and in Figure 1) was designed to carry out automatically measurements after applying deconvolution algorithms from DeconvolutionLab. The proposed procedure, in several steps, provides users the chance to manage a user interface to select a theoretical or an empirical PSF, choose between four deconvolution algorithms and set values for iteration, positivity constraint and regularization parameters.

More specifically, iterations were varied using 1, 2, 5, 10, 15 and 20 as set values, but they were even more augmented just in cases where the obtained morphology parameter values were keeping on getting closer to the expected ones. Although the maximum iteration value accepted is 1e6, the maximum iteration value used was 60 because after that the morphology values started to be unsatisfactory. Moreover, as the regularization parameter is able to be set between 0 and 1e6, it was varied establishing the next values: 0, 1e-15, 1, 10, 20, 50, 100, 1000, 10000, 100000, 1000000. Finally, positivity constraint activation and deactivation was combined to the already appointed parameter variations.

1° • Beads stack as well as PSFs stacks are loaded.

2° • The user choose a type of PSF, deconvolution algorithm and set of associated parameters. Then, during each execution:

.. • The slice where the maximum intensity values for beads was found in the original stack is set.

.. • An horizontal line selection is made along the width of the image in the XY-plane, crossing the middle of both beads (Figure 1(A)).

.. • An intensity profile is obtained through the previous selection (Figure 1(B)).

.. • Maximum intensity values and their positions are searched before and after of the middle of the intensity profile.

.. • Having found the two maximums, the exact minimum is searched between them.

.. • Intensities before and after the exact minimum (left and right beads) are fitted separately by a gaussian curve.

.. • In both cases, an approximated diameter is calculated by searching for an intensity value similar to the minimum, but placed on the opposite side.

.. • Two circular Regions of Interest (ROIs), previously manually defined, are loaded and used to measure the FWHM in Z-plane.

.. • A Result table is updated adding the obtained morphology, intensity and proximity parameter values.

.. • Moreover, output deconvolved stacks, which satisfy restrictions of minimum diameter and FWHM value, are saved as well as related intensity profiles.

3° • If the user wants to keep on working, the macro offers that chance by going back to the 2° step.

4° • The Result table is saved when the user decides to finish working.

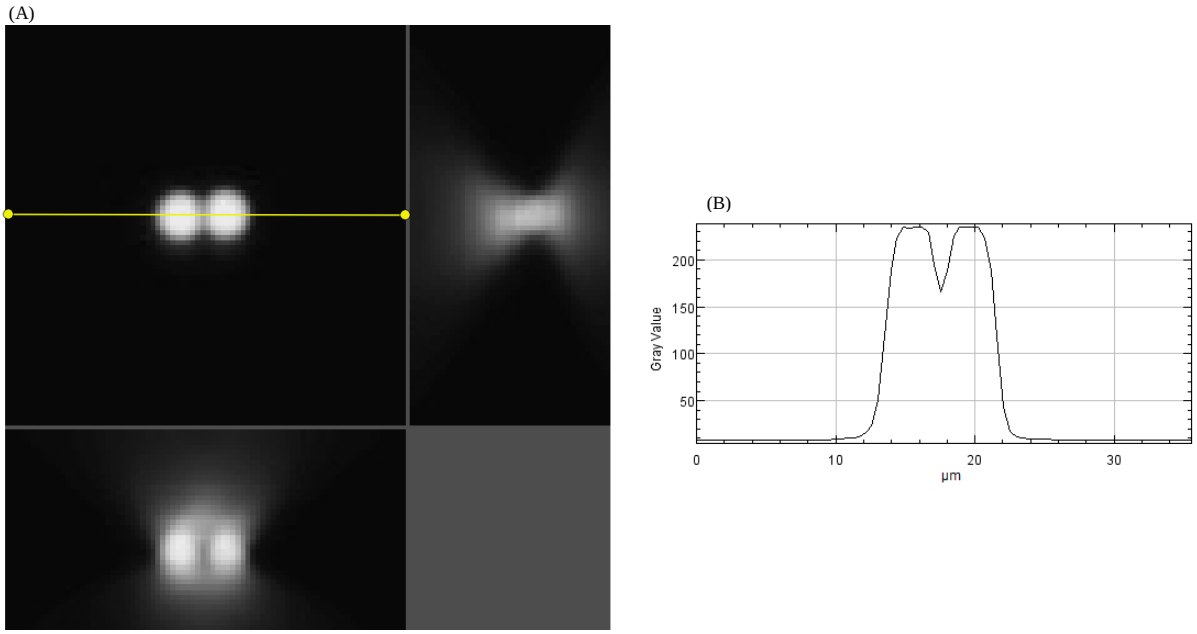

Figure 1 - **(A)** XY (top and left side), XZ (bottom) and YZ (top and right side) views of paired beads with a line selection. **(B)** Intensity profile of the selection in **(A)**. **(A)-(B)** are illustrative figures from pre-deconvolution measurements.

3.2 Procedure to analyze Icy's deconvolution algorithms through the morphology of the beads

An Icy procedure (depicted in the following chart) was designed to carry out measurements after applying deconvolution algorithms from MitivBlindDeconvolution. In this case, the PSF is developed by the plugin. Despite the fact that an Icy protocol could have been a good option to automatically test the performance, it was preferred to take advantage of the integrated FIJI software and the chance to use the same FIJI's measurement tools as before, converting the images to FIJI or Icy when it was necessary to use an Icy or FIJI plugin/tool.

1° • Beads stack is loaded.

2° • MitivBlindDeconvolution is opened and the user sets the images and parameters to be used.

.. • Deconvolved stack is convert to a FIJI object.

.. • Morphology, intensity and proximity parameters are measured by using a FIJI macro, adapted from the one described in 3.1 Section.

.. • A Result table is updated adding the obtained morphology, intensity and proximity parameter values.

.. • Moreover, output deconvolved stacks, which satisfy restrictions of minimum diameter and FWHM value, are saved. Related plot profiles are also saved.

3° • The user is able to save the Result table or go back to the 2° step to keep on working by resetting the parameters.

Iterations were varied using 1, 2, 5, 10, 15 and 20 as set values. They were increased in cases where the morphology parameter values obtained were keeping on getting closer to the expected ones, arriving to 30, 40, 50 or 100 iterations. Moreover, the regularization level was set using the next listed values: 0, 0.01, 0.5 and 1. Finally, enforce non-negativity activation and deactivation was combined to the already mentioned parameter variations.

At the end, parameters set in each deconvolution performance were manually added since they could not be detected by the FIJI macro.

3.3 Outcomes comparison

Deconvolution algorithms were executed using not only different parameter combinations (described in 3.1 and 3.2 sections), but also different types of PSF. Results attained were classified mainly regarding its changes in diameters in XY-plane and FWHM in Z-plane. In Figure 2 have been plotted the post-deconvolution intensity values belonging to the line selection in XY plus pre-deconvolution measurements. As can be observed, the best morphology outcomes obtained by Landweber and Tikhonov-Miller methods resulted in a huge reduction of the intensity values compared to pre-deconvolution measurements, whereas both Richardson-Lucy (RL) and Blind deconvolution algorithms resulted in the opposite effect, being more noticeable in the last one. The same behavior was detected in the intensity profiles through Z-plane of the ROIs selections of the beads. Figure 3 depicts one example corresponding to the left bead.

Tables 1 and 2 summarize the numerical morphology, intensity and proximity data belonging to the best performances as well as the parameters selected in each case. The analysis of Table 1 allows to determine that the best performances of the algorithms that did not yield an intensity decrease (shown in Table 2) included reduced FWHM between 5.3 and 4.2 µm from 6.8 µm and estimated diameters between 3.9 and 4.2 µm. Regarding to proximity parameters, those methods established a bigger separation between the maximum intensity values of the beads, increasing it from 1.8 µm onwards.

Based on the results obtained so far and visualizing the intensity plot profiles, which have been mentioned before, RL and Blind deconvolution algorithms using a theoretical PSF might be the methods that yield a deconvolved stack in which the beads resemble more to the actual morphology, increasing also the values of the intensity parameters. This is not surprising since the deconvolution reassigns intensities to the original distribution. The intensity difference between them might reside in the PSF used since a theoretical PSF developed by our research group was applied to DeconvolutionLab plugins while MitivBlindDeconvolution developed its own PSF using the image data.

Moreover, the shape of RL intensity profiles revealed that intensity is greater at the edges of the beads than in the center as it has been seen in deconvolved images showed in previous reports where polystyrene microspheres were also used (Conchello et al., 2005[20]; Soulez et al., 2012[21]). That feature is not clearly detected in Blind deconvolution.

Last but not least important, it worthwhile to mention that some issues have been found through the development of this process. Firstly, the regularization parameter in Tikhonov-Miller algorithm can be set from 0 to 1e6 but the resulting measurements are the same or exhibit almost imperceptible differences. Secondly, if a regularization parameter different of 0 is set in Blind deconvolution, the plugin does not work if the non-negativity is not enforced.

Finally, it is important to highlight that all of these analyses emphasize the importance of obtaining measurements to compare deconvolution algorithms by using patron specimens since if the analyses had carried out visually the deconvolution algorithms chosen could have been different, without realizing about morphology or intensity values changes.

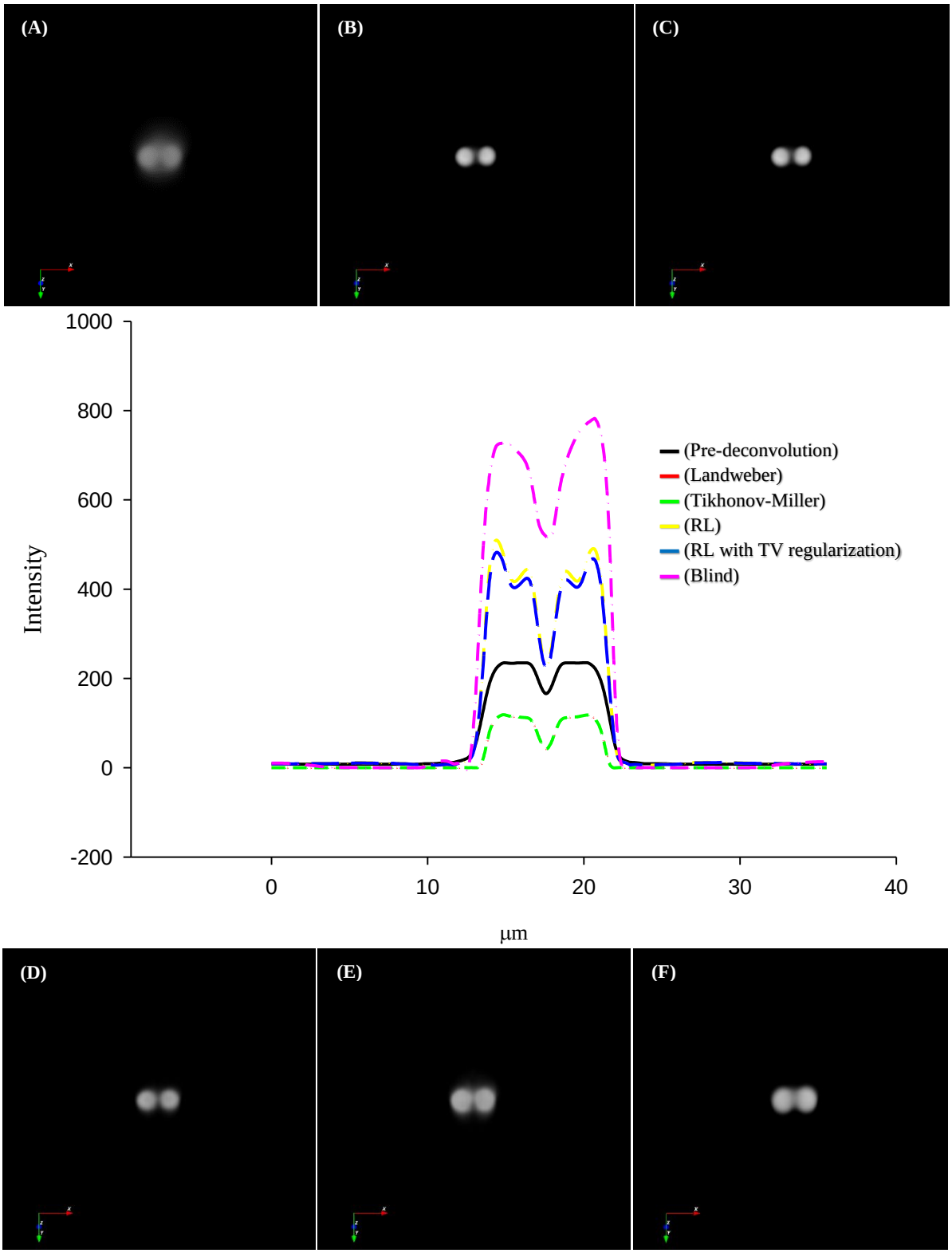

Figure 2 - Intensity profiles of the line selection crossing the beads in XY-plane. Landweber and Tikhonov used an empirical PSF while the rest used the theoretical one. **(A)-(F)** Pre-deconvolution, Landweber, Tikhonov-Miller, Richardson-Lucy, Richardson-Lucy with TV regularization and Blind Deconvolution 3D representations of the XY views using Icy.

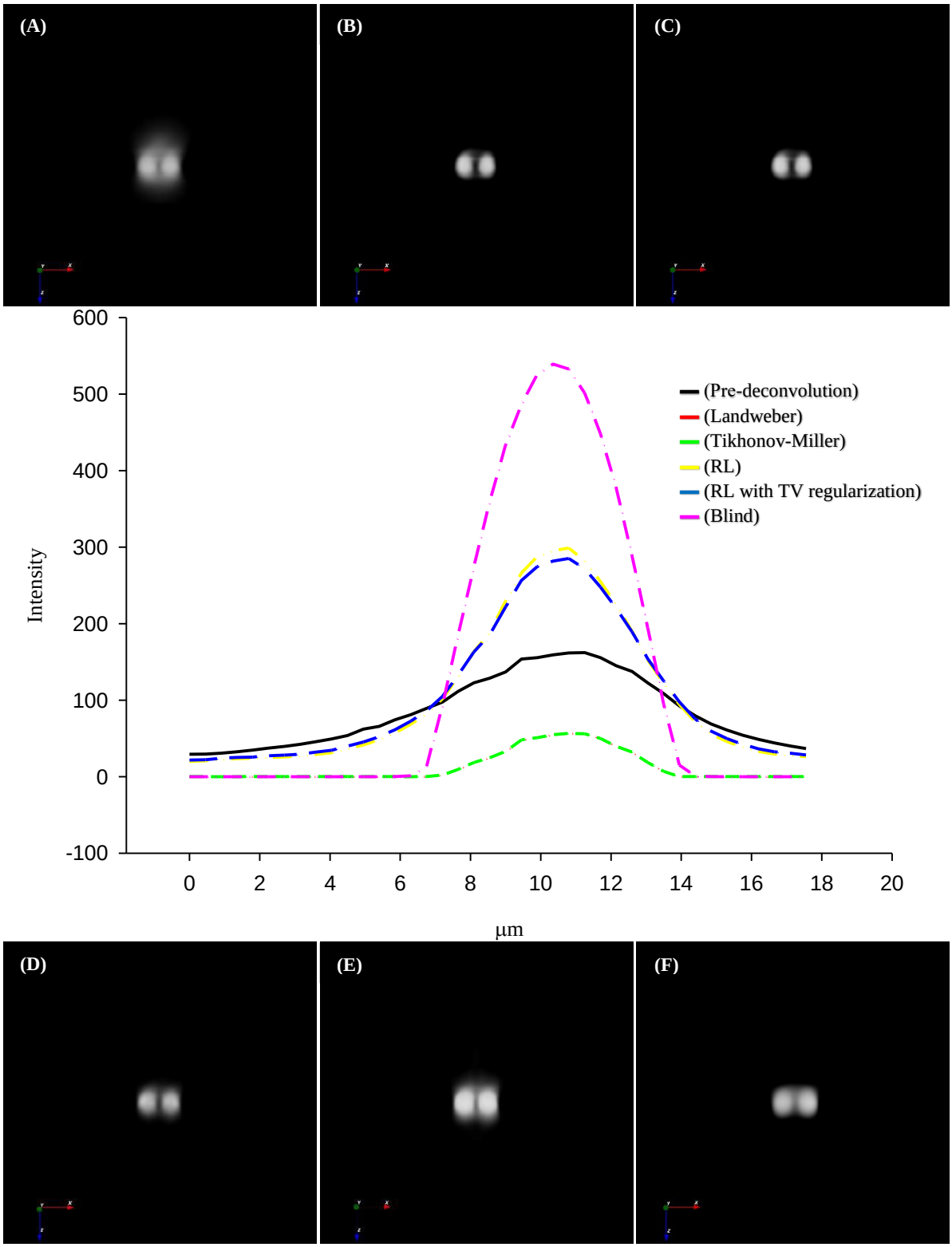

Figure 3 - Intensity profiles through Z-plane of the ROI selection of the left bead (Both beads presents similar plots). Landweber and Tikhonov used an empirical PSF while the rest used the theoretical one. **(A)-(F)** Pre-deconvolution, Landweber, Tikhonov-Miller, Richardson-Lucy, Richardson-Lucy with TV regularization and Blind Deconvolution 3D representations of the XY views using Icy.

Table 1 – Pre and post-deconvolution morphology parameter measurements.

	Positivity constraint	Regularization parameter	Iterations	Left bead		Right bead	
				Approximated diameter µm	FWHM µm	Approximated diameter µm	FWHM µm
Pre-deconvolution	-	-	-	3.723	6.846	3.723	6.616
Landweber	✓	-	10	3.900	3.716	4.000	3.596
Tikhonov-Miller	✓	0	10	3.900	3.716	4.000	3.596
Richardson-Lucy	-	-	60	4.255	4.901	4.182	5.157
RL with TV regularization	✓	0	50	4.255	5.071	4.182	5.330
Blind deconvolution	✓	0.01	25	3.900	4.206	4.182	4.247

Table 2 – Pre and post-deconvolution intensity and proximity parameter measurements.

	Left bead			Right bead			Distance between maximum intensity values XY µm
	Maximum intensity XY	Maximum intensity Z	Difference: maximum intensity XY and minimum intensity between beads	Maximum intensity XY	Maximum intensity Z	Difference: maximum intensity XY and minimum intensity between beads	
Pre-deconvolution	235	164.144	69	235	162.474	69	4.050
Landweber	118.897	56.409	77.272	118.226	56.586	76.601	5.400
Tikhonov-Miller	118.897	56.409	77.272	118.226	56.586	76.601	5.400
Richardson-Lucy	509.860	298.766	278.138	489.361	297.283	257.639	6.300
RL with TV regularization	482.466	285.164	257.636	465.891	284.083	241.060	6.300
Blind deconvolution	727.287	539.124	208.085	782.484	559.301	263.282	5.850

3.4 Deconvolution algorithms applied to colon tissue stacks

Based on the outcomes previously presented, the set of algorithms, parameters and PSF which revealed an acceptable performance (See RL and Blind Deconvolution outcomes in Table 1) were applied to 3D colon tissue images from BALB/c mice. These images were modified before deconvolution by using a self-developed photobleaching correction macro. The aim of this stage of the work was to test if combinations that restored the beads morphology and intensities can be applied to the colon tissue images, resulting in upgrades easily detectable at first glance.

Colon crypt structures were processed by applying RL and Blind deconvolution (Figures 4 and 5) but in RL the number of iterations was reduced to 10 because the number used for beads (60) caused shade off stacks. Intensity plots profiles were obtained by using a line selection in the original stack as well as in RL and Blind deconvolved stacks. The ones shown in Figures 4 and 5, from top to bottom, belongs to measurements carried out in the slices number 1, 20 and 40, respectively. Intensity values were increased at the same time as the number of the slice, denoting the crypts edges. In particular, the stacks deconvolved using RL method displayed better performance, always increasing the intensity value difference between the maximums on the edges and the middle of the crypt. The improvement was noticeable in the last slice of non-pathological stacks where the crypt could not be detected in the profile related to the original stacks, but it might be visualized using RL deconvolution.

As was already described in the introduction section, digital deconvolution methods, properly applied, are essential to enable the achievement of suitable detection and quantification of morphological alterations and autofluorescence intensities of objects of interest: the colon crypts. Thus, regarding the results obtained so far, RL algorithm and a suitable parameter setting could be applied to our 3D sets of images since visually improvements were detected. Those eye naked improvements were also quantitatively confirmed by intensity measurements.

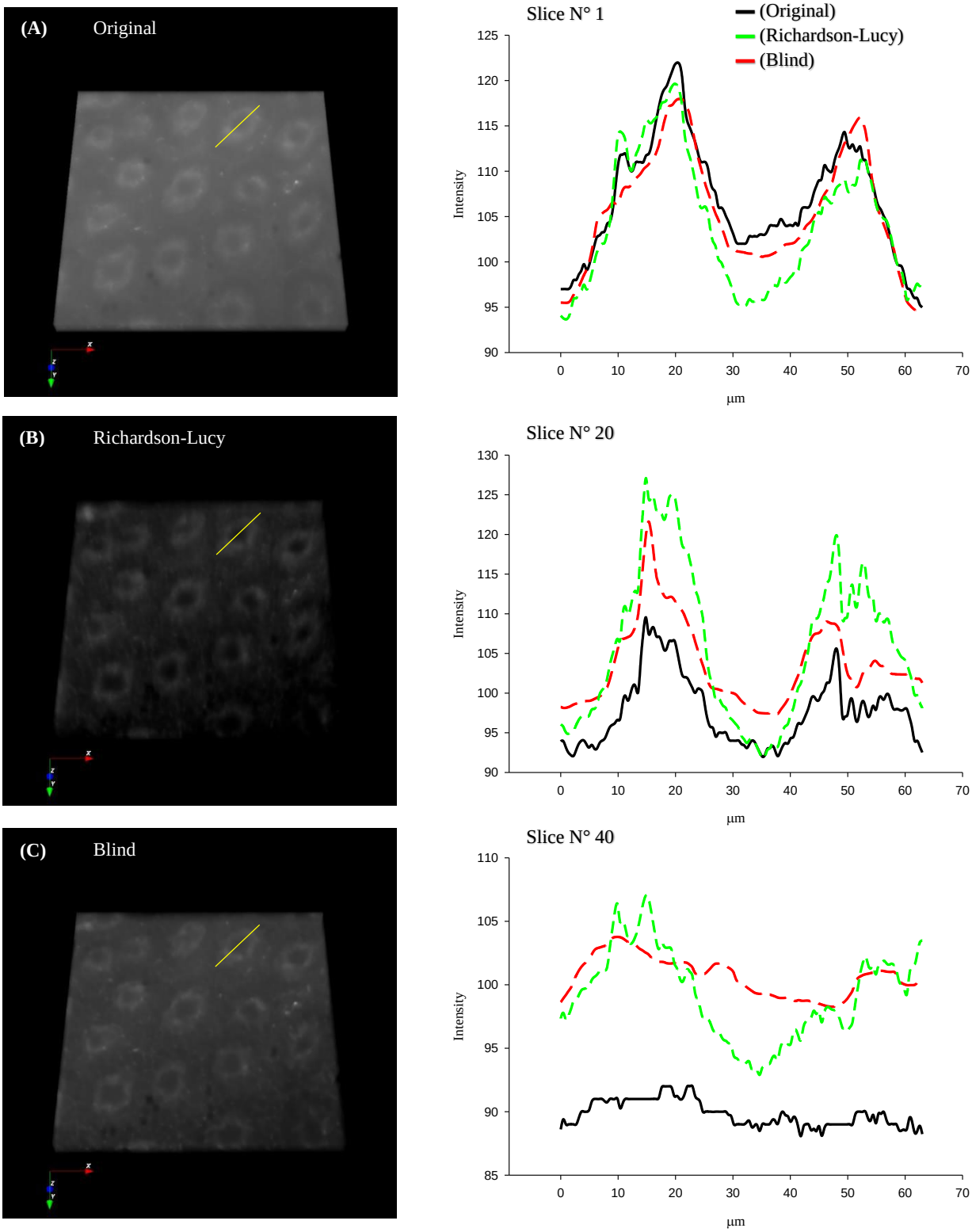

Figure 4 – Left: **(A)-(C)** Original, RL and Blind deconvolved non-pathological colon tissue stacks and line selections. Right: Intensity plot profiles of the line selections in **(A)-(C)**. (From top to bottom: Slices N°s 1, 20 and 40). Deconvolution parameters were set as described in Table 1.

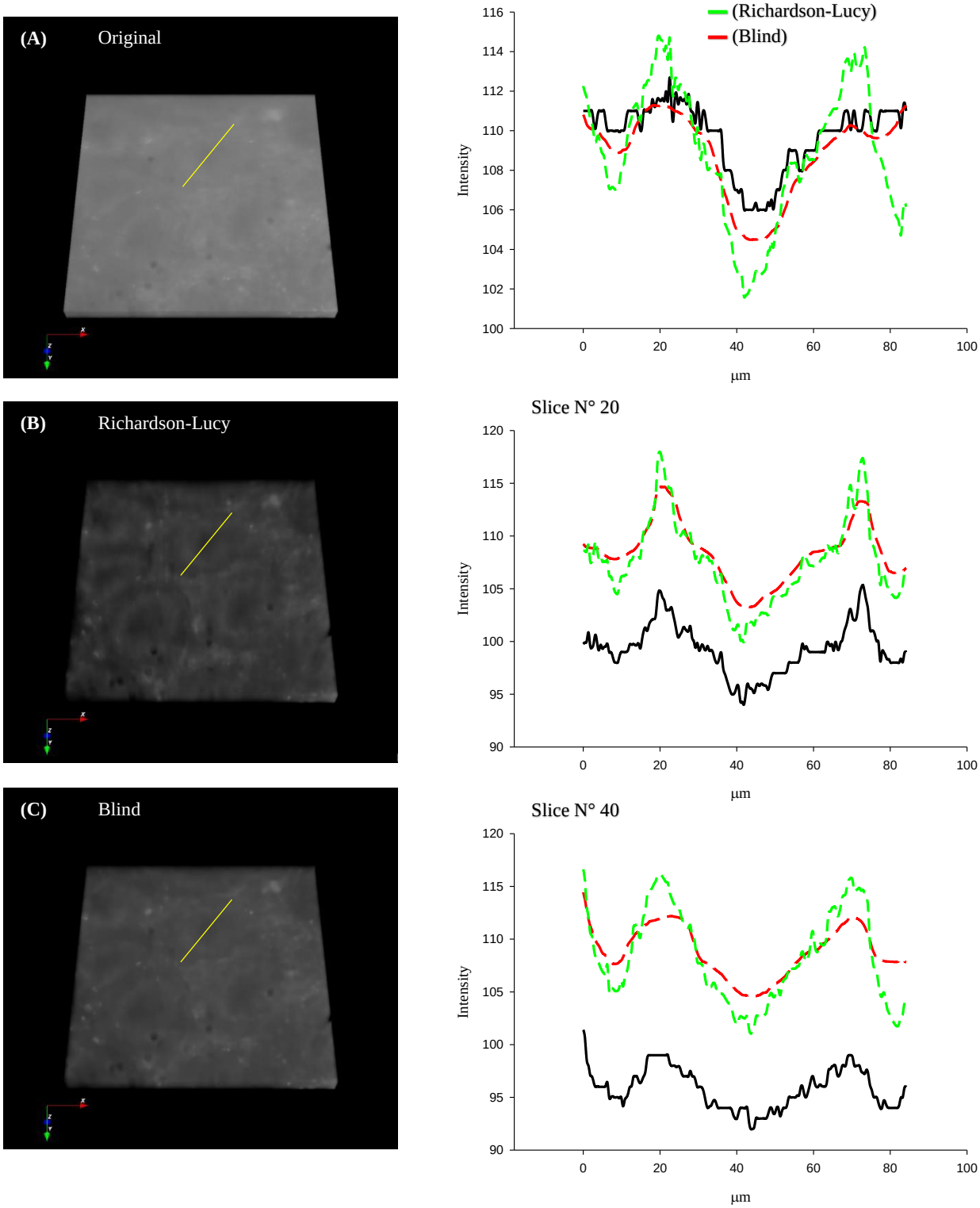

Figure 5 – Left: **(A)-(C)** Original, RL and Blind deconvolved pathological colon tissue stacks and line selections. Right: Intensity plot profiles of the line selections in **(A)-(C)**. (From top to bottom: Slices N°s 1, 20 and 40). Deconvolution parameters were set as described in Table 1.

4. CONCLUSIONS

The developed procedures are tools that allow users to easily and quickly test deconvolution algorithm performances by using a 3D beads image as patron specimens. The approach also offers the chance to introduce parameter variations as well as the PSF type, getting as a result a full set of morphology, intensity and proximity parameter data, which are saved in a file. By analyzing such parameter values it is possible to compare if the beads morphology are restored to the original size, intensity is increased and the resolving power is improved (distance between beads).

Valuable quantitative outcomes were obtained regarding to beads stack, achieving a suitable morphology restoration, increasing intensity signal and improving the resolving power, using RL and Blind deconvolution algorithms as well as theoretical PSFs. Moreover, the same algorithms and the same or similar parameter set could be applied to colon tissue stacks, obtaining adequate qualitative and quantitative outcomes and enabling to use the 3D images as initial stacks to perform 3D segmentation or quantification. Despite that, it should be taken in mind that different tissues can exhibit intensity differences regarding the beads used as patron, so the parameters must be carefully selected and adjusted in each case.

Even more, it is interesting to highlight that the procedure was fully developed using Open Source software and there are many deconvolution plugins available, although we only tested two of them. Thus, it is worthwhile to exploit the chance to test them by using the procedures described in the present report.

Finally, as we are looking for the development of a completely automatized method, future works will be addressed to the advantage of the integrated system of FIJI into Icy to write an Icy script able to test the performance of the deconvolution algorithms from both software during the same analyses. The aim will be to obtain a single data table for all deconvolution algorithms tested.

ACKNOWLEDGMENTS

PICTO UNER-INTA-CAFEGS; Contract grant number: 2009-209; Contract grant sponsor: PIO CONICET-UNER Res: 4337/15; Contract grant number: N8 14620140100004 CO).

REFERENCES

[1] Mcnally, J. G., Karpova, T., Cooper, J. and Conchello, J. A., “Three-Dimensional Imaging by Deconvolution Microscopy”, Methods 19, 374 (1999).

[2] Biggs, D. S. C., “Clearing Up Deconvolution”, Biophotonics, 4 (2004).

[3] Sibarita, J., “Deconvolution Microscopy”, Adv Biochem Engin/Biotechnol 95, 201–203 (2005).

[4] Sarder, P. and Nehorai, A., “Deconvolution Methods for 3-D Fluorescence Microscopy Images”, IEEE Signal Processing Magazine, 32–45 (2006).

[5] Scientific Volume Imaging, Deconvolution - Visualization – Analysis, The Netherlands, http://svi.nl/

[6] AutoQuant Deconvolutiom, http://www.mediacy.com/autoquantx3

[7] Schneider, C.A., Rasband, W.S. and Eliceiri, K.W., "NIH Image to ImageJ: 25 years of image analysis", Nature Methods 9, 671-675 (2012).

[8] Schindelin, J., Arganda-Carreras, I. and Frise, E., "Fiji: an open-source platform for biological-image analysis", Nature methods 9(7), 676-682 (2012).

[9] de Chaumont, F., Dallongeville, S., Chenouard, N., Hervé, N., Pop, S., Provoost, T., Meas-Yedid, V., Pankajakshan, P., Lecomte, T., Le Montagner, Y., Lagache, T., Dufour, A. and Olivo-Marin, JC., "Icy: an open bioimage informatics platform for extended reproducible research", Nature Methods 9, 690-696 (2012).

[10] Griffa, A., Garin, N. and Sage, D., "Comparison of Deconvolution Software in 3D Microscopy", G.I.T. Imaging & Microscopy, 43 (2010).

[11] Vonesch, C., Terrés Cristofani, R. and Schmit, G., "DeconvolutionLab - 3D deconvolution package for microscopic images" Biomedical Image Group (BIG), EPFL, Switzerland, http://bigwww.epfl.ch/algorithms/deconvolutionlab/

[12] Soulez, F., Denis, L., Tourneur, Y. and Thiébaut, É., "Blind Deconvolution of 3D Data in Wide Field Fluorescence Microscopy", 9th IEEE International Symposium on Biomedical Imaging (ISBI), 1735–1738, (2012). https://mitiv.univ-lyon1.fr/software/tutorial.html

[13] Burger, M., [Inverse Problems], Institut fur Numerische und Angewandte Mathematik, 1-78 (2007).

[14] van Kempen, G. M. P., van Vliet, L. J., Verveer, P. J. and van der Voort, H. T. M., "A quantitative comparison of image restoration methods for confocal microscopy", Journal of Microscopy 185, 354–365 (1997).

[15] Dey, N., Blanc-Feraud, L., Zimmer, C., Roux, P., Kam, Z., Olivo-Marin, J. C. and Zerubia, J., "Richardson-Lucy algorithm with total variation regularization for 3D confocal microscope deconvolution", Microscopy Research and Technique 69(4), 260–6 (2006).

[16] Castleman, K. R., [Digital Image Processing], Prentice Hall, 363 (1996).

[17] Molecular ProbesTM – Invitrogen detection technologies, FluoSpheres® Fluorescent Microspheres, Product Information (2005). https://tools.thermofisher.com/content/sfs/manuals/mp05000.pdf

[18] Bianchi, M., Adur, J., Izaguirre, M. F., Viale, S., Cesar, C. L. and Casco, V. H. "Endothelin-2 Differential Expression in Normal and Early-Stages of Colon Cancer Development", Journal of Cancer Therapy 4, 26–33 (2013).

[19] Vicente, N. B., Diaz-Zamboni, J. E., Adur, J. F., Izaguirre, M. F., Galetto, C. D. and Casco, V. H., "Development of a semi-automatic algorithm for deconvolution and quantification of three-dimensional microscopy images", Acta Microscopica 19(3), 328–336 (2010).

[20] Conchello, J. and Lichtman, J. W., "Optical sectioning microscopy", Nature Methods 2(12), 920-931 (2005).

[21] Soulez, F., Denis, L., Tourneur, Y. and Thiébaut, É., "Blind Deconvolution of 3D Data in Wide Field Fluorescence Microscopy", 9th IEEE International Symposium on Biomedical Imaging (ISBI), 1735–1738 (2012).